Effective mass enhancement and ultrafast electron dynamics of Au(111) surface state coupled to a quantum well

A. Varykhalov,[1] F. Freyse,[1,2] I. Aguilera,[3] M. Battiato,[4] M. Krivenkov,[1,2] D. Marchenko,[1] G. Bihlmayer,[3] S. Blügel,[3] O. Rader,[1] and J. Sánchez-Barriga[1,*]

[1]*Helmholtz-Zentrum Berlin für Materialien und Energie, Elektronenspeicherring BESSY II, Albert-Einstein-Strasse 15, 12489 Berlin, Germany*

[2]*Institut für Physik und Astronomie, Universität Potsdam, Karl-Liebknecht-Strasse 24/25, 14476 Potsdam, Germany*

[3]*Peter Grünberg Institut and Institute for Advanced Simulation, Forschungszentrum Jülich and JARA, D-52425 Jülich, Germany*

[4]*School of Physical and Mathematical Sciences, Nanyang Technological University, Nanyang Link 21, 637371 Singapore, Singapore*

(Received 23 October 2019; accepted 5 February 2020; published 19 March 2020)

We show that, although the equilibrium band dispersion of the Shockley-type surface state of two-dimensional Au(111) quantum films grown on W(110) does not deviate from the expected free-electron-like behavior, its nonequilibrium energy-momentum dispersion probed by time- and angle-resolved photoemission exhibits a remarkable kink above the Fermi level due to a significant enhancement of the effective mass. The kink is pronounced for certain thicknesses of the Au quantum well and vanishes in the very thin limit. We identify the kink as induced by the coupling between the Au(111) surface state and emergent quantum-well states which probe directly the buried gold-tungsten interface. The signatures of the coupling are further revealed by our time-resolved measurements which show that surface state and quantum-well states thermalize together behaving as dynamically locked electron populations. In particular, relaxation of hot carriers following laser excitation is similar for both surface state and quantum-well states and much slower than expected for a bulk metallic system. The influence of quantum confinement on the interplay between elementary scattering processes of the electrons at the surface and ultrafast carrier transport in the direction perpendicular to the surface is shown to be the reason for the slow electron dynamics.

DOI: 10.1103/PhysRevResearch.2.013343

I. INTRODUCTION

The Au(111) surface state is one of the most prominent examples of Shockley-type surface states [1–4]. It is supposed to have an ideal parabolic band dispersion which is well described in terms of the free-electron-like approximation and a spin-orbit splitting on a scale of ∼100 meV which is caused by the Rashba-Bychkov effect [5,6] due to the high atomic number of Au [7,8]. Recently, an alternative description of the Au(111) surface state in the framework of topological theory of solids was proposed [9]. Based on the connectivity of the surface state to the bulk bands far above the Fermi level and relying on the parity analysis of the calculated band structure [9], the Au surface state was identified as topologically nontrivial owing to the predicted Z_2-type invariants of Au [9]. Although the model appears elegant, it can be applied only conditionally because without an artificial increase in spin-orbit coupling strength [9], bulk Au(111) does not exhibit a continuous band gap along the time-reversal-symmetric direction of its surface Brillouin zone [10]. This fact, in turn, precludes a topological description from the dispersion of the Au(111) surface state. Especially for metals, the situation is nevertheless controversial as in the most general case the surface-state deviation from a parabolic band dispersion and its connectivity to the bulk bands do not necessarily imply topological protection [11]. An important example is the Rashba-split surface state of Ir(111) where the connectivity and parity of the bands resemble those of a topological system [12,13].

In this paper, we experimentally follow the dispersion of the Au surface state (SS) beyond the Fermi level (E_F), finding a remarkable deviation of the Au SS band dispersion from the expected free-electron-like behavior. We show that in a purely two-dimensional Au(111) film forming a quantum cavity grown on W(110), the SS can couple to quantum-well states (QWSs) residing inside the cavity and, as a result of the interaction of QWSs with the substrate, the SS acquires a significant renormalization of its effective mass. Our main finding is a kink structure in the energy-momentum dispersion $E(\mathbf{k})$ of the SS which is observed as a deviation from a naturally parabolic band which is demonstrated to be not related to topological properties but—even for thick quantum films—to the substrate. We further show that such coupling requires proximity of the SS to QWSs in energy-momentum space and, hence, the kink vanishes at small thickness (i.e., small width of

*Corresponding author: jaime.sanchez-barriga@helmholtz-berlin.de

the quantum well). As the kink resides within the unoccupied band structure, we use time- and angle-resolved photoemission (tr-ARPES) to access the band dispersion above E_F. The signatures of the coupling are also evidenced by our measurements of the ultrafast electron dynamics, which reveal that the renormalized SS and QWSs behave as dynamically locked electron populations exhibiting universal relaxation times significantly slower than expected for a bulk metallic system.

II. METHODS

We performed tr-ARPES experiments using linearly polarized 1.5-eV pump and 6-eV probe femtosecond (fs) laser pulses. The pulses were generated with a homemade Ti:sapphire fs oscillator coupled to an ultrafast amplifier laser system (RegA, Coherent) operated at 150-kHz repetition rate. The time delay Δt between pump and probe pulses was varied using an optical delay stage. The time resolution of the experiment was ~200 fs, and the pump fluence ~100 μJ/cm^2. Additional synchrotron-based ARPES measurements were carried out using linearly polarized undulator radiation at the U125-2-PGM beamline of BESSY-II in Berlin. Photoelectrons were detected with a Scienta R4000 analyzer at the RGBL-2 end station, and the base pressure of the experimental setup was better than 1×10^{-10} mbar. The angular and energy resolutions of the photoemission experiments were 0.1° and 20 meV, respectively. Au(111) quantum films were grown by deposition of 1–16 nm of Au on W(110) as described elsewhere [14]. High structural quality and homogeneity of the Au films were proved for thicknesses down to 1 nm by the observation of QWSs in the band structure using synchrotron radiation with photon energies above 60 eV. Laterally anisotropic strain relief patterns were observable by scanning tunneling microscopy (STM) at the surfaces of the films. Density functional theory (DFT) calculations were carried out within the all-electron full-potential linearized augmented-plane-wave formalism as implemented in the FLEUR [15] code. We used the Perdew-Burke-Ernzerhof functional, an angular momentum cutoff of $l_{max} = 10$ in the atomic spheres, and a plane-wave cutoff of 3.5 bohr^{-1}. Strain was simulated in all directions by rescaling the lattice constant. All calculations were performed for a freestanding 4-nm-thick Au slab taking spin-orbit coupling effects self-consistently into account. STM studies were conducted with an Omicron VT STM using a polycrystalline tungsten tip prepared as detailed elsewhere [16].

III. RESULTS AND DISCUSSION

A. Equilibrium band structure

Figure 1 provides information on electronic and structural properties of gold quantum films grown on W(110) using ARPES [Figs. 1(a) and 1(b)], low-energy electron diffraction (LEED) [Fig. 1(c)] (along with a sketch of the surface Brillouin zone (SBZ) of Au(111) and W(110) [Fig. 1(d)]), and STM [Figs. 1(e) and 1(f)].

Figure 1(a) shows the SS of a 7-nm-thick Au(111) quantum film grown on W(110) as seen by ARPES in equilibrium (6-eV probe photon energy and no pump photons) along the

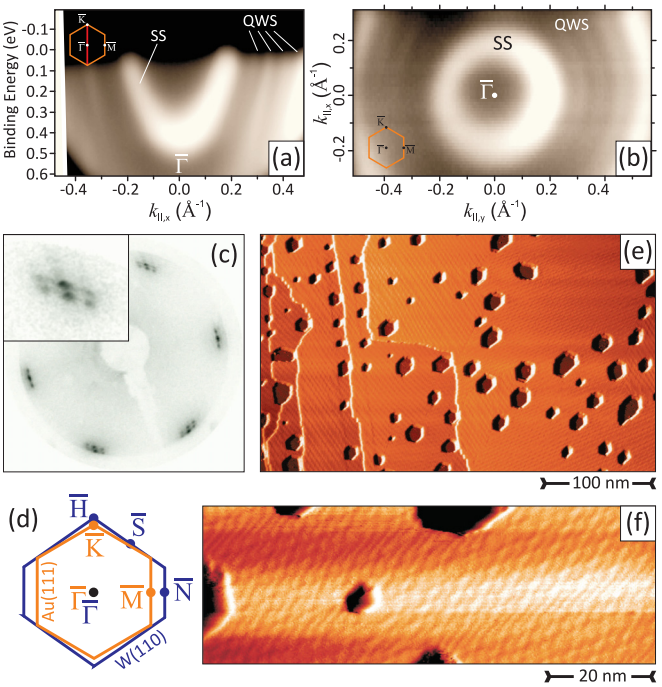

FIG. 1. Gold quantum films on W(110). (a) Au(111) SS of a 7-nm-thick film measured in equilibrium by ARPES at 6-eV photon energy. The multiple sharp bands next to it are QWSs occurring due to perpendicular-to-the-surface confinement of *sp* electrons. (b) At the Fermi surface, both SS and QWSs form onionlike perfectly concentric contours. (c) Low-energy electron diffraction reveals sharp spots of Au(111) surrounded by a spatially anisotropic superstructure originating from a herringbone reconstruction ($22\sqrt{3}$) modified by the strain induced from the substrate. (d) Sketch of the surface Brillouin zone of Au(111) (orange) and W(110) (blue) in mutual correspondence. (e) and (f) STM images. In (f), a zoom in on the herringbone-derived reconstruction is shown.

$\overline{\Gamma}$-$\overline{K}$ direction of the Au(111) SBZ [Fig. 1(d)]. The parabolic dispersion of the SS with the band bottom located at the $\overline{\Gamma}$ point of the SBZ and at ~0.43 eV binding energy is clearly visible. The bands next to the SS correspond to QWSs [14,17–22] occurring due to confinement of *sp* electrons in the potential well of the film.

The Fermi surface map in Fig. 1(b) shows a characteristic onionlike arrangement of sharp QWSs around the circular contour of the SS confirming the excellent structural quality of the quantum cavity. The homogeneous thickness of the Au film is also revealed by our STM images [Figs. 1(e) and 1(f)]. In particular, the dark hexagonal spots are surface features of only 1 to 2 monolayers (MLs) deep. In agreement with previous studies on Au quantum films [23], the Rashba-type spin-orbit splitting of the SS is not observed. We attribute this effect to an enhanced electron scattering at a network of surface distortions occurring due to strain, which is induced in the Au film by the low-symmetric W(110) substrate. Such dislocations might be responsible for lateral modulations of the electron wave function [24,25] and for the quenching of chiral orbital angular momentum of SS electrons [26], resulting in the vanishing spin splitting of Au SS. The dislocations occur as arrays in domains with different orientations [Fig. 1(e)] and

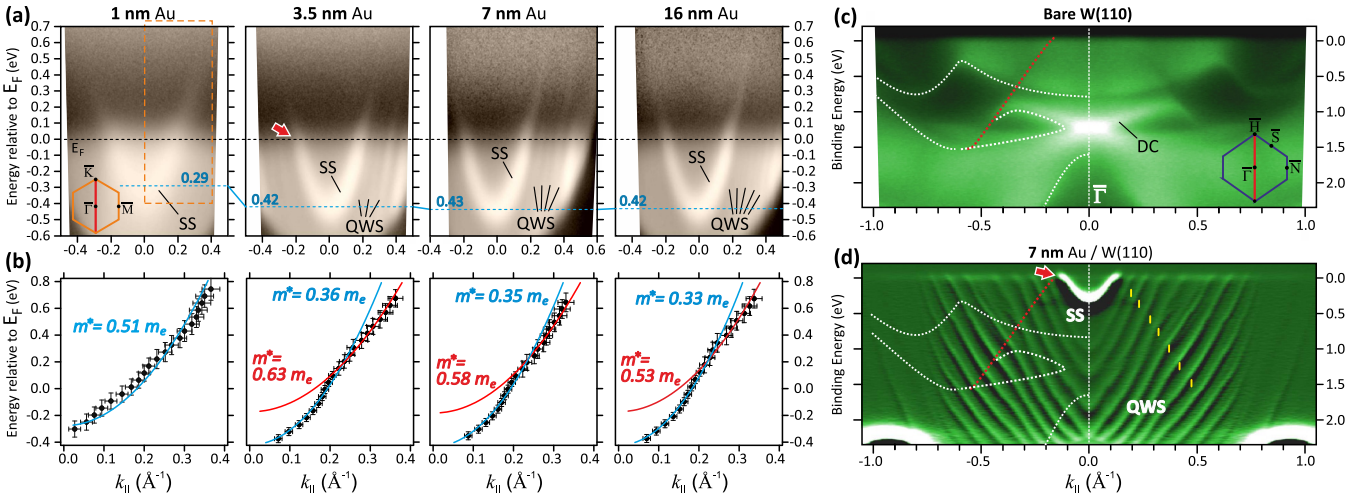

FIG. 2. (a) From left to right, tr-ARPES spectra of Au(111) quantum films of different thicknesses (1, 3.5, 7, and 16 nm) measured at $\Delta t = 0$. The energy-momentum dispersions of the surface state and quantum-well states are labeled as SS and QWS, respectively. (b) Corresponding band dispersions of Au SSs extracted from each panel in (a). The kink structure in the SS dispersion corresponds to an enhancement of the effective mass from ∼0.36–0.33m_e (blue lines) to ∼0.63–0.53m_e (red lines). (c) and (d) Band structures of (c) bare W(110) and (d) a 7-nm-thick Au film on W(110) measured with synchrotron radiation at 62-eV photon energy. The linearly dispersing band edge of W (red dashed line) causes kinks in the QWS bands (yellow ticks). It is also responsible for the kink in the SS due to SS-QWS coupling (see the text for details). White dashed lines mark the edges of the bulk W gap projected onto the (110) surface. The directions of the surface Brillouin zones of Au(111) and W(110) along which the band structures are sampled are indicated with red solid lines in the insets of (a) and (c), respectively.

have a periodicity of ∼25–30 Å as seen from the zoomed STM image shown in Fig. 1(f). The superstructure can be identified as a reshaped herringbone $(22\sqrt{3})$ reconstruction. Interestingly, we observe the dislocations more ordered than in earlier STM works [27]. Their well-defined periodicity is also confirmed by the perfectly ordered superstructural constellations seen by LEED [Fig. 1(c)].

B. Kink structure above E_F

Figure 2(a) shows the energy-momentum band dispersion of Au SS and QWSs measured by tr-ARPES at $\Delta t = 0$ fs for different widths of the quantum well. The unoccupied part of the band structure is now transiently populated with excited electrons and can be accessed directly. Whereas for a narrow potential well [1-nm film, left panel in Fig. 2(a)], a parabolic dispersion of the Au SS is seen, a deviation from this behavior can be identified with increasing quantum-well thickness.

In particular, at energies of ∼0.15 eV above E_F, the SS dispersion exhibits a kink structure and the electron group velocity decreases, evidencing a significant enhancement of the effective mass. The accurate extraction of the photoemission peaks along with parabolic fits of the band dispersion [Fig. 2(b)] reveals that due to the kink structure the effective mass of the SS increases by about a factor of 2 within the band itself, i.e., from ∼0.33 to 0.36m_e (blue lines) to ∼0.63 to 0.53m_e (red lines). Here, m_e denotes the free-electron mass. Interestingly, at 1-nm thickness [left panels in Figs. 2(a) and 2(b)], the effective mass of the whole SS band increases up to ∼0.51m_e. We attribute this effect to the influence of strain, which, in addition, causes the energy shift of the SS dispersion [horizontal blue dashed lines in Fig. 2(a)] and the surface distortions responsible for the broadening of the SS peaks.

C. Relevance of QWSs for the kink structure

The overall behavior of the energy-momentum dispersion of the SS seen in Figs. 2(a) and 2(b) indicates that QWSs and their coupling to the SS are highly relevant for the appearance of the kink structure. Indeed, the width of the quantum cavity defined by the Au thickness determines the electron confinement and, hence, the discrete energy spectrum of QWSs [see, e.g., Figs. 2(c) and 2(d) where the band structures of bare W(110) and a 7-nm-thick Au film grown on W(110) are compared]. One can, thus, assume that, at a certain thickness, the QWS band residing closer to the border of the surface-projected band gap of Au(111) approaches the SS band localized therein and couples to it causing the kink. This effect is qualitatively illustrated in Fig. 3, which shows a schematic of the electronic band structures of thin [Fig. 3(a)] and thick [Fig. 3(b)] Au(111) quantum films. In line with this assumption, it was earlier shown that the SS of Cu(111) can gain effective mass even due to coupling to nonconfined states of the bulk [28], however, no kink structure exists in the bulk limit [9,28], and the mass enhancement is much stronger in the case of coupling to QWSs as shown in the present paper.

D. Influence of strain on the SS and its topological character

To understand whether the kink structure is inherent to the quantized electronic structure of Au(111), we performed model DFT calculations for a 4-nm-thick Au slab as shown in Fig. 4. In the course of the simulation, we changed the binding energy of the SS via small variations of the lattice constant, simulating in this way the strain induced in the Au film by the W substrate. This allowed us to move the Au SS band close to the region above E_F near the border of the Au(111) surface band gap and, accordingly, closer to the QWS band with the

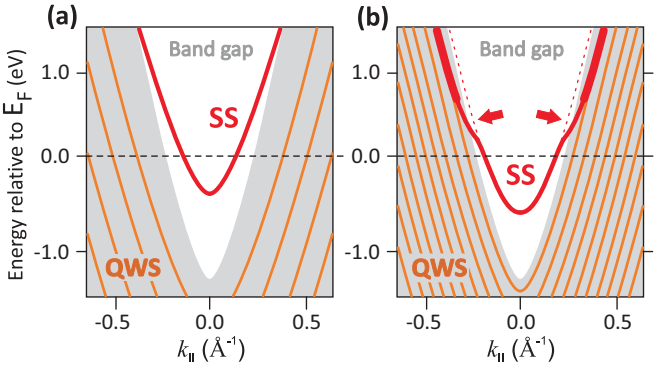

FIG. 3. Sketch illustrating the coupling between the Au(111) SS and the QWSs in Au quantum films. (a) For extremely thin films, the spectrum is discrete, but SS (red line) and QWS bands (orange lines) have large separations in energy-momentum space, and the coupling is weak. (c) For thicker Au quantum films, the number of QWS bands increases, reducing the separation and enhancing the coupling thereby giving rise to a kink structure in the SS dispersion (red arrows). The vanishing spin-orbit splitting is based on the experimental findings (see the text).

lowest binding energy. One can see that, although the energy spectrum of QWSs is less perturbed by such a change, the SS band dispersion reacts very sensitively [29].

Figure 4 shows four panels corresponding to different grades of strain induced in the Au slab: zero strain [Fig. 4(a)], expansive strain of +1% [Fig. 4(b)], compressive strain of −5% [Fig. 4(c)], and extreme compressive strain of −10% [Fig. 4(d)]. Strain not only causes an energy shift of the SS dispersion and a change in its effective mass, but also a reduction of the spin splitting. These findings, which are qualitatively in line with our experimental results of Fig. 2, are related to the fact that strain directly affects orbital hybridization [24,25]. The effect also manifests at energies of ∼2–4 eV above E_F [region marked with orange dashed rectangles in Fig. 4(a)] where there is strong deviation of the free-electron-like character of the SS dispersion. In particular, one of the spin subbands of the Rashba-split SS is more affected by the interaction with the QWS which is closest to it in energy-momentum space, pinpointing the importance of the coupling. Conversely, from the results in Fig. 4, one can also see that the SS kink at ∼0.15 eV above E_F is negligible. This result is surprising considering that the calculation captures qualitatively most of the relevant aspects of the experimental band dispersion of Fig. 2, namely, (i) the energy shift of the SS, (ii) the change in its effective mass, (iii) the vanishing spin splitting, and (iv) the importance of the coupling between SS and QWS bands. Therefore, we conclude that the origin of the kink structure in Fig. 2 must be necessarily related to the quantized electronic structure of Au(111), but in a much more complex way, as we will discuss further below.

We also point out that the calculation in Fig. 4 shows no global band-gap opening at high energy as evidenced in the entire Brillouin zone by the fact that QWSs do not disperse in the direction perpendicular to the surface. This situation is also the case of an extremely strained (−10%) Au film [Fig. 4(d)], which exhibits a local band-gap opening only in the region marked with an orange circle in Fig. 4(d). Although 10% strain is not achievable in real samples, taking into account that the $\overline{\Gamma}$-$\overline{M}$ direction of the Au(111) SBZ connects two time-reversal invariant momentum points, this result clearly underlines that the observed connectivity of the bands in the marked circle is not related to topological properties but to the fact that the Au SS lies in an inverted band gap [1].

E. Influence of the substrate band structure

Coming back to the kink structure observed in Figs. 2(a) and 2(b), the fact that it is not reproduced by our calculations in Fig. 4 indicates that the electronic band structure of the underlying W(110) substrate must play a decisive role. To verify the effect of the W substrate, in Fig. 2(d), we display the overall band structure of ∼7-nm-thick Au on W(110) measured with synchrotron light at a photon energy of 62 eV along the $\overline{\Gamma}$-$\overline{K}$ direction of the Au(111) SBZ [equivalent to the $\overline{\Gamma}$-$\overline{H}$ direction of the W(110) SBZ as sketched in Fig. 1(d)]. Very clearly, the dispersions of the QWS bands exhibit kinks (marked by yellow ticks) along the borders of the surface-projected band gap of W(110) [Fig. 2(c)] due to enhanced interface reflectivity of the standing electron waves [14]. The linearly dispersing band of W at the border of the gap is marked by the red dashed lines in Figs. 2(c) and 2(d). It

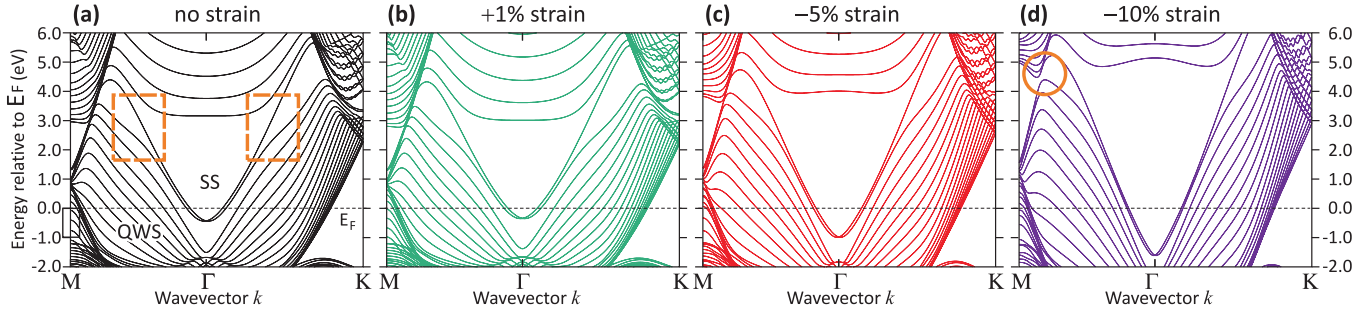

FIG. 4. DFT calculations of the band structure of a 4-nm-thick Au slab subjected to different grades of strain. (a) No strain, (b) expansive strain of +1%, (c) compressive strain of −5%, and (d) extreme compressive strain of −10%. In (a), the calculated momentum splitting of spin subbands of the SS is ∼0.035 Å^{-1}. Strain causes an energy shift of the SS band dispersion, a change in its effective mass, and a reduction of the spin splitting. The deviation from free-electron-like behavior in the SS dispersion becomes more pronounced close to the region where the SS connects to QWS bands [orange dashed rectangles in (a)]. For an extremely strained Au film in (d), the opening of an inverted band gap along the time-reversal-invariant direction $\overline{\Gamma}$-$\overline{M}$ (orange circle) is shown by the connectivity of the bands.

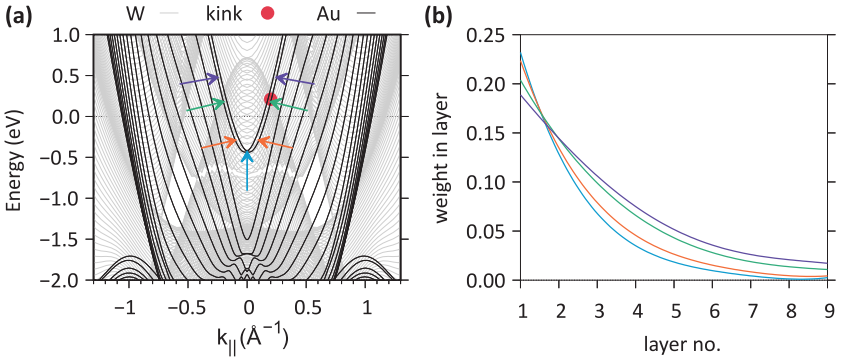

FIG. 5. (a) DFT calculation of bulk W projected on the surface Brillouin zone (gray lines) compared to the bands of a 4-nm Au slab (black lines) as in Fig. 4(a) in the direction $\overline{\Gamma}$-$\overline{\mathrm{K}}$. (b) **k**-dependent decay of the SS wave function within the 4-nm slab. The red solid circle in (a) indicates the position of the experimentally observed kink. The colored arrows in (a) indicate the energy-momentum points at which the curves in panel (b) are obtained.

crosses the Au SS dispersion just above E_F at nearly the same k value where the kink structure appears (red arrow in figure).

We propose that the SS kink structure, similar to the kinks in the QWS bands, occurs due to the influence of this linear W(110) band [which is actually an edge of the projection of the W bulk bands onto W(110)]. In Fig. 5(a), we superimpose the band structure of the 4-nm slab of Fig. 4(a) on a calculation of the bulk W substrate (gray lines). Despite the large lattice mismatch between Au(111) and W(110) [Fig. 1(d)], this procedure can give a good account of the effects of the QWS near $\overline{\Gamma}$. With a red circle, we highlight the approximate position of the experimentally observed kink. It is very apparent that this position coincides with the crossing of the Au SS with the linear band of W that corresponds to the red dashed line in Fig. 2(d). This theoretical result supports the experimental evidence that the presence of the substrate plays a decisive role in the appearance of the kink. To further verify the role of QWS bands, we plot, in Fig. 5(b), the calculated decay of the SS wave function within several layers from the surface of the 4-nm slab. The curves are taken for the SS at four different momenta as marked by the colored arrows in Fig. 5(a). It is clear that as we move away from the $\overline{\Gamma}$ point, the proximity to QWS bands increases and, in consequence, the SS decay length becomes longer due to the coupling to QWSs.

Therefore, we conclude that the influence of the W(110) band structure on the Au SS must be necessarily mediated by QWSs, which transfer the band-structure information from the buried Au/W interface to the surface of the Au film [14]. This exclusive role of QWSs, which is inherent to the Au band structure, is further supported by the absence of a mass-renormalization kink in the SS dispersion for very thin films [left panels in Figs. 2(a) and 2(b)], meaning that, in this different scenario, the overall coupling picture described in Fig. 3 still holds.

F. Revealing the importance of SS-QWS coupling via electron dynamics

To further investigate if the coupling between different states is important for the appearance of the kink, we examined the ultrafast temporal evolution of the transient electron populations above E_F within SS and QWS bands as shown in Fig. 6 for different widths of the quantum cavity. In particular,

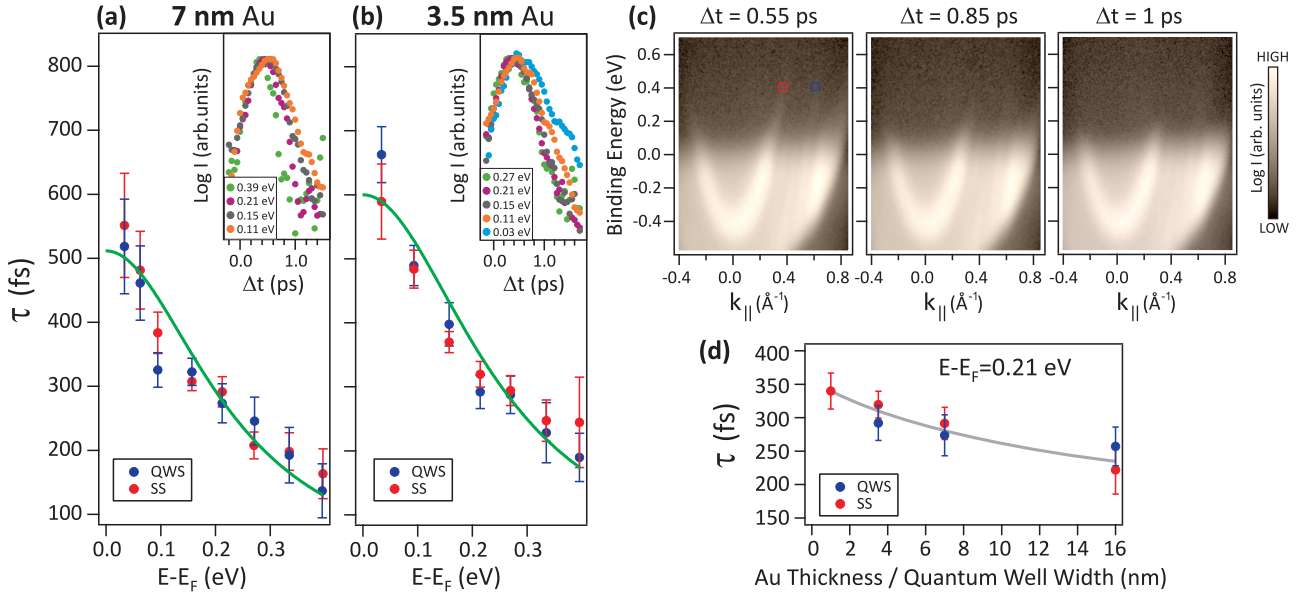

FIG. 6. (a) and (b) Decay constants of the surface state [red (light) color] and quantum-well states [blue (dark) color] for Au quantum films of (a) 7-nm and (b) 3.5-nm thicknesses. The corresponding time-resolved intensities as a function of time delay at different selected energies are shown in the insets. The data were extracted from small energy-momentum windows, such as the ones shown in (c). Green (light) solid lines are fits to the data (see the text). (c) From left to right, tr-ARPES dispersions at selected time delays ($\Delta t = 0.55$, 0.85, and 1 ps) after optical excitation. (d) Thickness dependence of the decay times at an energy of 0.21 eV above E_F. The gray solid line is a guide to the eye.

this type of measurement allows us to understand whether the coupling influences the relevant scattering channels responsible for charge and energy transfer between different states and whether there is a simultaneous thermalization of carriers. In Figs. 6(a) and 6(b), we show the dependence of the decay time-constants τ on the energy of excited electrons above E_F for two selected thicknesses of the quantum cavity (7 and 3.5 nm, respectively). The decay constants were extracted separately for the SS and QWS bands (red and blue symbols, respectively) from the exponential decay seen in the time evolution of the tr-ARPES intensities (an example for the SS at selected energies is shown in the corresponding insets). The tr-ARPES intensities were integrated at each time delay within several small energy-momentum windows distributed at different energies within the SS and QWS bands. An example of such windows is shown in Fig. 6(c), which displays snapshots of the band structure at selected time delays for a 7-nm-thick film.

From the disappearance of the tr-ARPES intensity above E_F, one can see that the system is almost back to equilibrium after $\Delta t \sim 1$ ps. Moreover, excited electrons within the SS and QWS bands decay synchronously with nearly identical decay constants, behaving as dynamically locked electron populations, which evidences the signatures of the coupling between the different states. This behavior suggests that interband scattering processes of the electrons at the surface are one of the key mechanisms underlying the simultaneous thermalization. Note that, by thermalization, we refer to the situation in which the whole electronic system is described by a global Fermi-Dirac distribution.

More in detail, as seen from Figs. 6(a) and 6(b), the energy dependence of τ for Au SS and QWSs follows a universal monotonic behavior that can be described as $\tau \propto (E\text{-}E_F)^{-2}$ (green solid lines). This correspondence evidences the Fermi-liquid-like behavior of charge carriers [30,31] which is expected for hot electrons in metals [32]. However, the values of τ exceed, by far, the predicted decay times for the bulk system [33,34]. The decay-time τ according to Ref. [35] is given by $\tau^{-1} = \tau_l^{-1} + z^{-1}\tau_{FL}^{-1}$, where τ_l is an effective time constant related to the contributions of electron-phonon scattering as well as electron transport and τ_{FL} is the lifetime associated with Fermi-liquid behavior due to inelastic electron-electron scattering. Consistent with this, from the linewidth analysis near E_F, we derive an energy independent lifetime of $\sim(11 \pm 4)$ fs associated with elastic impurity scattering which contributes negligibly to the measured decay times. The scaling coefficient z was introduced for Au(111) films by Cao *et al.* [35] and determined as 6.5 in order to eliminate the discrepancy with jellium-model calculations by Quinn [31], providing, in this way, an estimation for τ_{FL} but not accounting for screening effects caused by Au 5*d* electrons. In our present paper, the best fit to the experimental data of Figs. 6(a) and 6(b) provides for the 7-nm (3.5-nm) film $\tau_l = 511(600) \pm 44(48)$ fs and $z = 27(38) \pm 5(7)$, which supports the description of Au quantum films on W(110) in the framework of the jellium model [31]. The fact that screening effects by Au *d* electrons are not taken into account make the model nevertheless applicable to our system since the *d* bands in quantum wells are suppressed due to electron confinement [23,36,37].

G. Transversal electron transport as a benchmark for the influence of the substrate band structure

Figure 6(d) displays the thickness dependence of the decay times extracted near the region of the kink structure at an energy of 0.21 eV above E_F. One can see that the decay times of SS and QWS bands increase with decreasing thickness. This behavior can also be noted in the energy dependence of the decay times when comparing Figs. 6(a) and 6(b). There are several effects that can explain this observation. One of them is the influence of ultrafast carrier transport (ballistic or diffusive) [38–41] from the surface to the bulk of the Au film with increasing thickness. However, the efficiency of these channels should be weak as no Au bulk states are observed in our photoemission spectra. In addition, as the SS is located within the surface-projected band gap of Au(111), there cannot be an electron transport channel from the SS to the bulk of the Au film without interband scattering because no Au bulk states are available inside the gap.

Alternatively, one might consider the opening up of electron transport channels from the surface of the Au film to the interface with the W substrate. It is known that this type of transversal transport can act as a net loss of electron population through the leakage of electrons towards the substrate. The efficiency of such process, however, ultimately depends on the electronic band-structure mismatch between overlayer and substrate. Therefore, in the most general case, this type of transport will be completely blocked in the region of energy-momentum space where there is a relative band gap of the substrate. For the Au SS within the region of the surface-projected gap, one can see by comparing Figs. 2(c) and 2(d) that near E_F there is a continuum of W bulk states available around $\overline{\Gamma}$. However, as the SS is strongly localized at the Au(111) surface, efficient electron transport directly from the Au SS towards the W substrate should result in faster decay times with decreasing thickness, in contrast to our observations in Fig. 6.

We do note that the continuum of W bulk states is also available for electron transport through QWSs, which due to crystal momentum conservation and the symmetry match of the propagating electrons [17,18] continue dispersing outside and near the edge of the W gap. Thus, it is clear that transversal electron transport from the surface of the Au film towards the W substrate is necessarily mediated by QWSs and that this process cannot proceed without interband scattering which is the main mechanism responsible for the simultaneous thermalization of SS and QWS bands. The fact that both aspects are critically important in the electron dynamics is in line with our conclusion that QWSs and their coupling to the SS are key ingredients for the influence of the W substrate in the appearance of the kink.

We can finally exclude any significant role of ultrafast longitudinal transport along the direction parallel to the surface in the dynamics. Considering the large ($\sim$300-μm) lateral spot size of the pump pulse and the estimated group velocity of SS electrons (<0.7 nm/fs), the lateral propagation range of excited electrons will not exceed 1.5 μm (even without taking into account the electron mean free path which is $\sim$200–300 Å at a given kinetic energy of 2 to 3 eV).

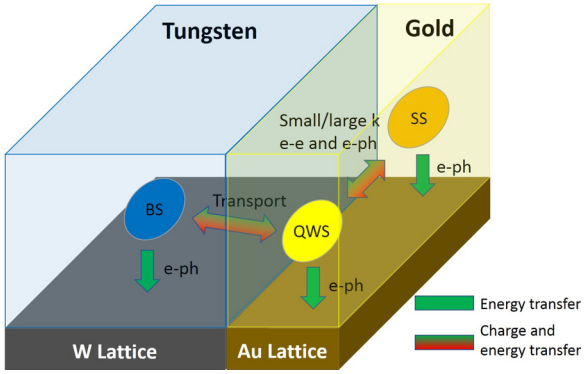

FIG. 7. Schematic of the main thermalization mechanisms observed in Au(111) quantum films grown on W(110). Three fundamentally different thermalization routes are highlighted: (1) electron-electron (*e-e*) scatterings, responsible for energy and charge transfer between SS and QWS bands; (2) electron-phonon (*e-ph*) scatterings, responsible for charge transfer between bands as well as energy dissipation into the lattice; and (3) transport from surface of the film towards the substrate, leading to both charge and energy transfer between QWS bands and a continuum of W bulk states (BS). Note how this transversal transport channel is blocked for the SS within the region of the surface-projected band gap of Au(111) (see the text).

H. Influence of quantum confinement on the thermalization time scales as a verification of the coupling scenario

In Fig. 7, we show a schematic which, on the basis of our present findings, summarizes the most important channels of ultrafast charge and energy transfer between different bands as well as their energy dissipation into the lattice. Interband transitions via electron-electron and electron-phonon scatterings are predominantly responsible for the overall transfer of charge and energy between SS and QWS bands. When the separation between SS and QWS bands in energy-momentum space increases and their coupling becomes weak [see Fig. 3(a)], the energy and charge transfer channels between SS and QWS bands become less effective because electron-electron and electron-phonon scatterings require larger k transfers with predominance of electron-electron scatterings the higher the energy. Note that, due to the presence of a surface band gap, intraband scattering would lead, instead, to different chemical potentials in the SS and QWS bands which is clearly not the case here.

In addition, quantization of electronic states with decreasing Au thickness in the direction perpendicular to the surface reduces the phase space for electron-electron scattering, causing the decay times to increase with decreasing thickness as seen in Fig. 6(d). Quantization effects also reduce the effectiveness of electron transport towards the substrate, which together with electron-phonon scatterings being responsible for the transfer of energy into the lattice, are the only two mechanisms relevant to the dynamics in the vicinity of E_F. The influence of these effects in the electron dynamics is consistent with the overall coupling scenario behind the origin of the kink structure discussed in previous sections.

It should be emphasized that, for the pump intensities employed here ($\sim 6.3 \times 10^8$ W/cm^2), no heating of the lattice itself needs to be considered [35]. In other words, the electron-phonon coupling strength, which has been shown to be rather independent of film thickness [42], is not affected by the pump excitation itself. Taking into account that the electron-phonon scattering time in Au is about 30 fs and that $\hbar\omega_D = 15$ meV where ω_D is the Debye frequency [30], we estimate that it will take about 420 fs for an electron to lose 0.21 eV. This timescale is clearly above the decay times seen in Fig. 6(d), and it cannot entirely explain the larger values of the effective time-constant τ_l extracted from Figs. 6(a) and 6(b). On one hand, this result highlights the impact of quantization effects on the efficiency of transversal electron transport near E_F, which is the main reason for the increasing values of τ_l with decreasing thickness. On the other hand, it also provides further evidence for the importance of electron-electron scattering which is, in any case, a slow channel of thermalization due to Auger-like secondary electron emission upon recombination of the hot electron with a hole [41].

IV. SUMMARY

In conclusion, the present results offer an alternative route to engineer the band dispersion of surface states in two-dimensional metallic systems where quantum-size effects are important. Using photoemission in combination with time, energy, and momentum resolution, we have accessed the band dispersion of the Shockley-type SS of two-dimensional Au(111) quantum films grown on W(110) above and below E_F. Our results show that the SS dispersion significantly deviates from the parabolic behavior expected for a free-electron-like system. The deviation appears more pronounced above E_F where we observe a kink structure that is consistent with a remarkable enhancement of the SS effective mass.

In combination with DFT calculations, we have analyzed various aspects that are relevant for the modification of the SS dispersion, namely, the impact of strain, the influence of the substrate band structure, and the crucial role of QWSs and their coupling to the SS for the appearance of the kink. Finally, we have provided further evidence for the decisive role of the substrate band structure and the overall coupling scenario behind the origin of the kink structure through direct measurements of the electron dynamics. These measurements also reveal a unique relationship between the decay timescales and the influence of quantum confinement on the efficiency of the relevant channels responsible for ultrafast charge and energy transfer following optical excitation. Our findings taken as a whole are relevant in the context of understanding the fundamental properties of surface states of quantum films grown on substrates and clearly demonstrate how the interplay between quantum confinement in the film and the electronic structure of the substrate determine the equilibrium and dynamical properties of the surface states.

ACKNOWLEDGMENTS

Financial support from the Impuls-und Vernetzungsfonds der Helmholtz-Gemeinschaft under Grant No. HRSF-0067 (Helmholtz-Russia Joint Research Group) is gratefully acknowledged. M.B. gratefully acknowledges financial support from the Nanyang Technological University, NAP-SUG.

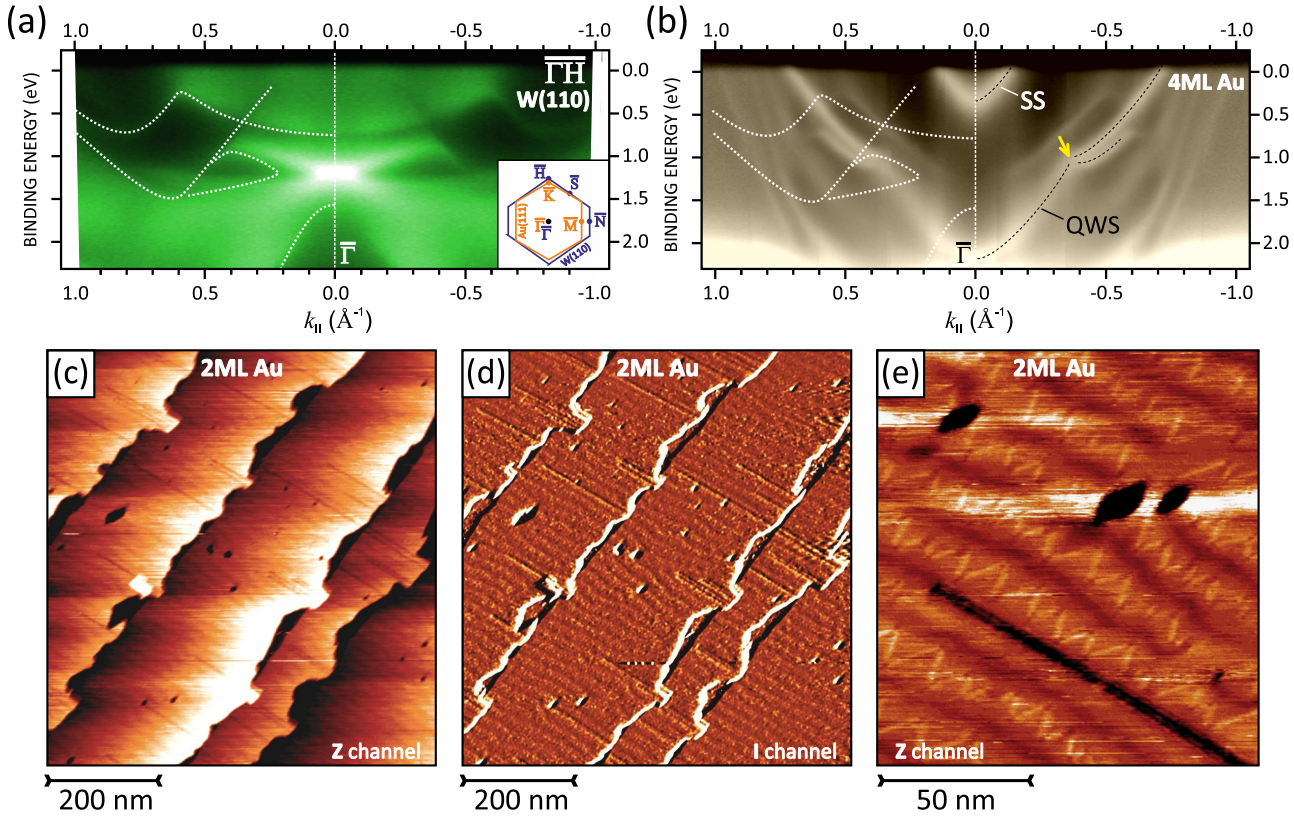

FIG. 8. Characterization of thin Au films grown on W(110). (a) and (b) Band structures of bare W(110) (a) and 1-nm thick Au film on W(110) (b) measured by ARPES along the $\overline{\Gamma}$-$\overline{\mathrm{H}}$ direction of the W(110) surface Brillouin zone (inset) using synchrotron radiation ($h\nu =$ 62 eV). A pronounced QWS band is seen in (b). Its dispersion is modified (yellow arrow) due to the interaction with tungsten bands (white dashed lines). The grayscale intensity in (b) is logarithmic. (c) and (d) Large-scale STM characterization of ∼2-ML-thick Au on W(110). Maps of topography (c) and variation of tunneling current (d) are presented. The film exhibits uniform thickness and strictly uniaxial strain relief pattern with transverse periodicity of 10−15 nm; (e) zoom into this pattern uncovers its complex zigzaglike inner morphology. Acquisition parameters: $V_t = +5$ mV, $I_t = 6$ nA.

APPENDIX

An important issue related to Au quantum films grown on W(110) and subjected to anisotropic strain due to low-symmetric tungsten face is the overall homogeneity and structural quality of the Au overlayer as well as the specific morphology of the strain relief. This is particularly important for the thinnest Au film studied in our paper (nominal thickness of 1 nm), which, in ARPES, exhibits a SS with the largest energy shift and peak broadening as compared to thicker Au films (Fig. 2).

We have extensively characterized the equilibrium band structure of Au films of various thicknesses grown on top of W(110) using synchrotron-based ARPES. To this end, we used larger excitation energies (e.g., $h\nu = 62$ eV) than in the case of the laser-based ARPES measurements to probe higher binding energies and to profoundly test quantization effects in the electronic structure of Au further away from the $\overline{\Gamma}$ point. Figures 8(a) and 8(b) show the band structure of bare W(110) [Fig. 8(a)] and a 1-nm-thick (4 ML) Au film grown on W(110) [Fig. 8(b)] sampled along the $\overline{\Gamma}$-$\overline{\mathrm{H}}$ direction of the W(110) SBZ [corresponding to the $\overline{\Gamma}$-$\overline{\mathrm{K}}$ direction of the Au(111) SBZ, see the inset of Fig. 8(a)]. In Fig. 8(b), apart from the broadened Au SS, a pronounced QWS band is clearly observed. At high binding energies, the dispersion of the QWS band is substantially affected (region marked with yellow arrow) by the interaction with W(110) bands (emphasized by white dashed lines), resulting in a modification of its nearly parabolic form [14]. At the same time, the appearance of a QWS band in the photoemission signal is clear and sharp. This, in turn, proves the very high structural quality and homogeneity of the 1-nm-wide quantum cavity. Indeed, the most important precondition for the existence of a QWS is the perfectness of the film surface/interface which is crucial for reflection and confinement of electrons in the film [17]. In addition, the binding energy of the QWS band provides important and accurate information on the thickness of the Au layer. Simulation of QWS energies in the framework of extended phase accumulation model [36,43] confirms the thickness of deposited gold as 4 ML (1 nm).

Further valuable insight on the structural quality of the Au film as well as on the strain acting in the film can be obtained by STM. Figures 8(c)–8(e) show STM results of a slightly thinner Au film (nominally deposited amount of Au was between 2 and 3 ML) than the one investigated in photoemission experiments (4 ML), however, for 4-ML Au, the results are qualitatively the same. Figures 8(c) and 8(d) display the results of a large-scale STM scan and confirm once again the homogeneous thickness of the Au layer. The

only steps seen in the images reproduce the morphology of wide and flat terraces of bare W(110) rather precisely and, hence, confirm layer-by-layer growth with uniform thickness [STM results of our comparative study for bare W(110) are not shown].

A uniaxial strain-relief pattern can be clearly observed at the surface of the film. It is better seen in Fig. 8(d) which displays the same area of the sample as in Fig. 8(c) but as a variation of tunneling current (which is more sensitive to small corrugations and fine-structural features). The strain relief pattern in the 1-nm-thick Au film is, however, different than in thicker Au overlayers. For thin Au, the relief pattern is strictly uniaxial and does not exhibit rotational domains as seen e.g., in Fig. 1(e). In addition, transverse periodicity (∼10–15 nm) of the relief structure at the surface is four to five times larger and has more complex morphology as compared to thick Au films [Fig. 1(f)]. Figure 8(e) shows a zoom onto the observed uniaxial strain relief pattern and uncovers its inner zigzag structure, which might be a precursor of the herringbone reconstruction in the ultrathin limit. The different and more pronounced character of the strain in the 1-nm-thick Au film is fully in line with the larger energy shift and substantial modification of the effective mass of the whole SS band ($m^* \sim 0.51 m_e$) [left panels in Figs. 2(a) and 2(b)].

[1] W. Shockley, Phys. Rev. **56**, 317 (1939).
[2] S. LaShell, B. A. McDougall, and E. Jensen, Phys. Rev. Lett. **77**, 3419 (1996).
[3] F. Reinert, G. Nicolay, S. Schmidt, D. Ehm, and S. Hüfner, Phys. Rev. B **63**, 115415 (2001).
[4] M. Hoesch, M. Muntwiler, V. N. Petrov, M. Hengsberger, L. Patthey, M. Shi, M. Falub, T. Greber, and J. Osterwalder, Phys. Rev. B **69**, 241401(R) (2004).
[5] E. I. Rashba, Fiz. Tverd. Tela (Leningrad) **2**, 1224 (1960) [Sov. Phys. Solid State **2**, 1109 (1960)].
[6] Y. A. Bychkov and E. I. Rashba, J. Phys. C: Solid State Phys. **17**, 6039 (1984).
[7] G. Bihlmayer, Y. M. Koroteev, P. M. Echenique, E. V. Chulkov, and S. Blügel, Surf. Sci. **600**, 3888 (2006).
[8] M. Nagano, A. Kodama, T. Shishidou, and T. Oguchi, J. Phys.: Condens. Matter **21**, 064239 (2009).
[9] B. Yan, B. Stadtmüller, N. Haag, S. Jakobs, J. Seidel, D. Jungkenn, S. Mathias, M. Cinchetti, M. Aeschlimann, and C. Felser, Nat. Commun. **6**, 10167 (2015).
[10] S. N. P. Wissing, C. Eibl, A. Zumbülte, A. B. Schmidt, J. Braun, J. Minár, H. Ebert, and M. Donath, New J. Phys. **15**, 105001 (2013).
[11] A. Varykhalov, D. Marchenko, J. Sánchez-Barriga, E. Golias, O. Rader, and G. Bihlmayer, Phys. Rev. B **95**, 245421 (2017).
[12] A. Varykhalov, D. Marchenko, M. R. Scholz, E. D. L. Rienks, T. K. Kim, G. Bihlmayer, J. Sánchez-Barriga, and O. Rader, Phys. Rev. Lett. **108**, 066804 (2012).
[13] J. Sánchez-Barriga, G. Bihlmayer, D. Wortmann, D. Marchenko, O. Rader, and A. Varykhalov, New J. Phys. **15**, 115009 (2013).
[14] A. Varykhalov, J. Sánchez-Barriga, A. M. Shikin, W. Gudat, W. Eberhardt, and O. Rader, Phys. Rev. Lett. **101**, 256601 (2008).
[15] www.flapw.de.
[16] A. Varykhalov, O. Rader, and W. Gudat, Phys. Rev. B **72**, 115440 (2005).
[17] J. J. Paggel, T. Miller, and T.-C. Chiang, Science **283**, 1709 (1999).
[18] R. K. Kawakami, E. Rotenberg, H. J. Choi, E. J. Escorcia-Aparicio, M. O. Bowen, J. H. Wolfe, E. Arenholz, Z. D. Zhang, N. V. Smith, and Z. Q. Qiu, Nature (London) **398**, 132 (1999).
[19] T. Miller, A. Samsavar, G. E. Franklin, and T. C. Chiang, Phys. Rev. Lett. **61**, 1404 (1988).
[20] P. Moras, G. Bihlmayer, P. M. Sheverdyaeva, S. K. Mahatha, M. Papagno, J. Sánchez-Barriga, O. Rader, L. Novinec, S. Gardonio, and C. Carbone, Phys. Rev. B **91**, 195410 (2015).
[21] A. Varykhalov, A. M. Shikin, W. Gudat, P. Moras, C. Grazioli, C. Carbone, and O. Rader, Phys. Rev. Lett. **95**, 247601 (2005).
[22] J. H. Dil, F. Meier, J. Lobo-Checa, L. Patthey, G. Bihlmayer, and J. Osterwalder, Phys. Rev. Lett. **101**, 266802 (2008).
[23] P. M. Sheverdyaeva, R. Requist, P. Moras, S. K. Mahatha, M. Papagno, L. Ferrari, E. Tosatti, and C. Carbone, Phys. Rev. B **93**, 035113 (2016).
[24] E. E. Krasovskii, Phys. Rev. B **90**, 115434 (2014).
[25] H. Ishida, Phys. Rev. B **90**, 235422 (2014).
[26] S. R. Park, C. H. Kim, J. Yu, J. H. Han, and C. Kim, Phys. Rev. Lett. **107**, 156803 (2011).
[27] T. Giela, K. Freindl, N. Spiridis, and J. Korecki, Appl. Surf. Sci. **312**, 91 (2014).
[28] A. A. Ünal, C. Tusche, S. Ouazi, S. Wedekind, C.-T. Chiang, A. Winkelmann, D. Sander, J. Henk, and J. Kirschner, Phys. Rev. B **84**, 073107 (2011).
[29] G. Neuhold and K. Horn, Phys. Rev. Lett. **78**, 1327 (1997).
[30] N. W. Ashcroft and N. D. Mermin, *Solid Sate Physics* (Holt, Rinehart, and Winston, New York, 1976).
[31] J. J. Quinn, Phys. Rev. **126**, 1453 (1962).
[32] E. Knoesel, A. Hotzel, T. Hertel, M. Wolf, and G. Ertl, Surf. Sci. **368**, 76 (1996).
[33] V. M. Silkin, P. Lazić, N. Došlić, H. Petek, and B. Gumhalter, Phys. Rev. B **92**, 155405 (2015).
[34] X. Cui, C. Wang, A. Argondizzo, S. Garrett-Roe, B. Gumhalter, and H. Petek, Nat. Phys. **10**, 505 (2014).
[35] J. Cao, Y. Gao, H. E. Elsayed-Ali, R. J. D. Miller, and D. A. Mantell, Phys. Rev. B **58**, 10948 (1998).
[36] A. M. Shikin, O. Rader, G. V. Prudnikova, V. K. Adamchuk, and W. Gudat, Phys. Rev. B **65**, 075403 (2002).
[37] D.-A. Luh, J. J. Paggel, T. Miller, and T.-C. Chiang, Phys. Rev. Lett. **84**, 3410 (2000).
[38] M. Battiato, K. Carva, and P. M. Oppeneer, Phys. Rev. Lett. **105**, 027203 (2010); Phys. Rev. B **86**, 024404 (2012).
[39] M. Battiato, P. Maldonado, and P. M. Oppeneer, J. Appl. Phys. **115**, 172611 (2014).
[40] J. Sánchez-Barriga, M. Battiato, E. Golias, A. Varykhalov, L. V. Yashina, O. Kornilov, and O. Rader, Appl. Phys. Lett. **110**, 141605 (2017).
[41] F. Freyse, M. Battiato, L. V. Yashina, and J. Sánchez-Barriga, Phys. Rev. B **98**, 115132 (2018).
[42] J. Hohlfeld, S.-S. Wellershoff, J. Güdde, U. Conrad, V. Jähnke, and E. Matthias, Chem. Phys. **251**, 237 (2000).
[43] A. M. Shikin, D. V. Vyalikh, G. V. Prudnikova, and V. K. Adamchuk, Surf. Sci. **487**, 135 (2001).